Steel and Composite Structures, Vol. 9, No. 5 (2009) 397-418
DOI: http://dx.doi.org/10.12989/scs.2009.9.5.397

Flexural behaviour and capacity of composite panels of light gage steel and concrete

L. Shi[1], Y. Liu[2]*, J. L. Dawe[1] and P. Bischoff[1]

[1]*Dept of Civil Engineering, Univ. of New Brunswick, Fredericton, NB, Canada*
[2]*Dept of Civil and Resource Engineering, Dalhousie Univ., NS, Canada*

(Received March 19, 2009, Accepted July 20, 2009)

Abstract. Eight panel specimens were tested in one-way bending to study the behaviour and capacity of composite slab joists consisting of cold-formed steel C-sections and concrete. Various shear transfer mechanisms were implemented on the C-section flange embedded in the concrete to provide the longitudinal shear resistance. Results showed that all specimens reached serviceability limit state while in elastic range and failure was ductile. Shear transfer achieved for all specimens ranged from 42 to 99% of a full transfer while specimens employed with shear transfer enhancements showed a greater percentage and therefore a higher strength compared with those relying only on surface bond to resist shear. The implementation of pre-drilled holes on the embedded flange of the steel C-section was shown to be most effective. The correlation study between the push-out and panel specimens indicated that the calculated moment capacity based on shear transfer resistance obtained from push-out tests was, on average, 10% lower than the experimental ultimate capacity of the panel specimen.

Keywords : composite; cold-formed steel; light gage; shear transfer; flexural capacity.

1. Introduction

Design and construction of systems consisting of steel beams and girders in composite with concrete slabs has been a common practice in bridge engineering (AASHTO 2005, Greiner, *et al*. 2002) and building construction (Ekberg and Schuster 1968, Porter and Ekberg 1976) for several decades. The most widely employed system incorporated hot-rolled steel sections with shear transfer between the concrete slab and beam provided by welded headed shear studs (Culver and Coston 1961, Badie, *et al*. 2002, El-Lobody and Lam 2002). The cold-formed steel composite concrete floor systems have been commonly used in North America in small commercial and residential constructions in which concrete is poured onto a corrugated cold-formed steel sheet, which is in turn connected to the supporting beams through shear connectors, often shear studs (Erdélyi and Dunai 2009). The use of this type of cold-formed steel composite slab system with shear studs as shear connectors has been well established in North America with detailed design guidelines available in both American (ASCE specification 1984) and Canadian (CSA S136-01 2001) design standards. In this research, attention was given to another type of application where light gage cold-formed steel sections are in direct composite with a relatively thin concrete slab forming a longitudinal one-way member in bending. They are referred to as light gage steel concrete (LGSC) panels. The first record of the application of LGSC panels appeared in the early 1980s (United

* Associate Professor, Corresponding Author, Email: yi.liu@dal.ca

States Patent and Trademark Office 2003). Aside from the structural advantages of composite members, LGSC panels are relatively lightweight and can be readily stored, transported, handled and installed. They can be pre-fabricated under factory conditions and later assembled onsite. Despite many advantages, there is little available technical literature and scientific documentation regarding reliable analysis and design procedures for LGSC panels. Only in recent years has this type of composite structure begun to attract some deserved research attention (Lakkavalli and Liu 2006). One essential element of these composite systems is the shear connection between the steel and the concrete. Since the steel sections are light gage and the slab is relatively thin, the welding of shear studs is not applicable. Shear connectors in the form of fasteners proposed by Hanaor (2000) exhibited good capacity for shear transfer in experiments. But failure was often caused by pullout of the fasteners used to attach the light gage steel section to the embedded connection and the installation of these fasteners is costly. A review of a database provided by the United States Patent and Trademark Office (2003) showed that many attempts have been made to simplify shear connection design during the past fifteen years in an effort to industrialize the manufacture of LGSC panels. However, little information is available on the performance of the different types of connection that have been proposed.

Unlike conventional LGSC panels where a concrete slab is in contact with the top surface of a flange of a light gage steel section, the LGSC panels studied in this research were formed by partially embedding the flange of a light gage steel C-section into a concrete slab. Partially embedding the steel section was intended to utilize the surface bond between steel and concrete to assist in shear transfer. The concrete formed around the compressive flange of the steel section would also provide lateral support and thus prevent the compressive buckling of the thin steel in this region. To increase the shear transfer capacity, particularly after the concrete cracks, two shear transfer enhancements including predrilled holes and bent-up tabs were proposed to be employed on the embedded flange of the steel section. To verify the effectiveness of the shear transfer enhancements, their shear transfer capacities and their effect on the flexural behaviour of the composite structure needed to be first experimentally investigated and determined. An experimental program was therefore designed and carried out to study the efficacy of various shear transfer mechanisms in both push-out tests and flexural tests of panel specimens. The correlation between push-out and panel specimens was discussed. Recommendations on the proposed shear transfer mechanisms for potential industry implementation were provided.

2. Experimental program

The experimental program involved the testing of eight LGSC panel specimens and twenty companion push-out specimens. Light gage cold-formed steel C-sections were used in the casting of all specimens. Three types of shear transfer mechanism between the steel and concrete were considered in both panel and push-out specimens. Details of the mechanisms are provided in the next section. The panel specimens were tested to study the overall behavior and capacity of LGSC panels whereas push-out tests were used to evaluate the transfer capacity of the individual shear transfer mechanisms.

2.1 Panel specimen tests

2.1.1 Test specimens

Table 1 shows the details of panel specimens. All specimens were tested under uniform lateral pressure

with a span of 2330 mm. As shown in Fig. 1, each specimen consisted of a solid 2438 mm long by 1219 mm wide by 64 mm thick concrete slab with two partially embedded cold-formed steel C-sections conforming to CSA S136-01 (2001). The specimens were fabricated by embedding two nominally 1524 mm thick steel C-sections, spaced 609 mm apart, to a depth of 38 mm into a 64 mm thick concrete slab. C-sections measuring 41 × 203 mm were used in the five specimens, LSCP1 to LSCP5, whereas C-sections measuring 41 × 152 mm were used in the remaining three specimens. Standard 152 × 152 × MW18.7 × MW18.7 welded wire mesh was placed immediately above the C-section flanges and secured in place while casting.

The shear transfer mechanisms used in these specimens at the steel-concrete interface are indicated in Table 1 and shown in Fig. 2. These mechanisms included Type A with direct surface bonding between the embedded flange of the steel section and the surrounding concrete; Type B which consisted of 25 mm predrilled holes at a spacing of 100 mm on the embedded flange; and Type C which included bent-up triangular tabs formed from X-shaped cross-cuts made in the embedded flange at a spacing of 100 mm. For specimen LSCP5, the embedded flange was coated with grease in an attempt to measure the effect of debonding between the steel and the concrete. Specimens LSCP7 and LSCP8, which were nominally identical, were tested to check that the test set-up was capable of delivering consistent results.

All panel specimens were cast and cured for at least 28 days before testing. For ease of construction, specimens were fabricated in the inverted position. Ready-mix concrete, with a maximum aggregate size of 19 mm, was used in all specimens.

2.1.2 Test set-up and procedure

Fig. 3 shows the test set-up. Uniform lateral pressure was simulated by a pneumatic pressure bag built to exert a lateral pressure up to 80 kPa. An existing test frame, which had been formerly used to test masonry panels, was modified to be used to test all specimens in a vertical position. Test specimen end supports were designed to ensure simply supported boundary conditions. Detailed lateral and vertical support arrangements are shown in Figs. 4 and 5, respectively. In the vertical direction, each end of a specimen was housed in a built-up steel channel section which was in turn held in position using a steel beam with a weld attached round steel rod extending the full length of a specimen. Free rotation of the ends of a panel specimen was achieved through the rotation of the steel rod inside semicircular pipe sections attached to the upper and lower panel supports. At the lower support, to simulate ideal pinned conditions, a trolley roller system was employed to minimize the friction and the consequent end

Table 1 Description of panel specimens

Specimen	Concrete slab			Steel C-section (16 gage)		Shear transfer mechanism
	Dimensions (mm)	f'_c (MPa)	f_t (MPa)	Dimension (mm)	f_y (MPa)	
LSCP1	2438 × 1219	33.8	3.49	2- 41 × 203	299.8	Type-A
LSCP2	2438 × 1219	33.8	3.49	2- 41 × 203	299.8	Type-B
LSCP3	2438 × 1219	33.8	3.49	2- 41 × 203	299.8	Type-C
LSCP4	2438 × 1219	36.6	3.70	2- 41 × 203	299.8	Type-B
LSCP5	2438 × 1219	36.6	3.70	2- 41 × 203	299.8	Type-B greased
LSCP6	2438 × 1219	37.2	4.25	2- 41 × 152	306.5	Type A
LSCP7	2438 × 1219	37.2	4.25	2- 41 × 152	306.5	Type B
LSCP8	2438 × 1219	37.2	4.25	2- 41 × 152	306.5	Type B

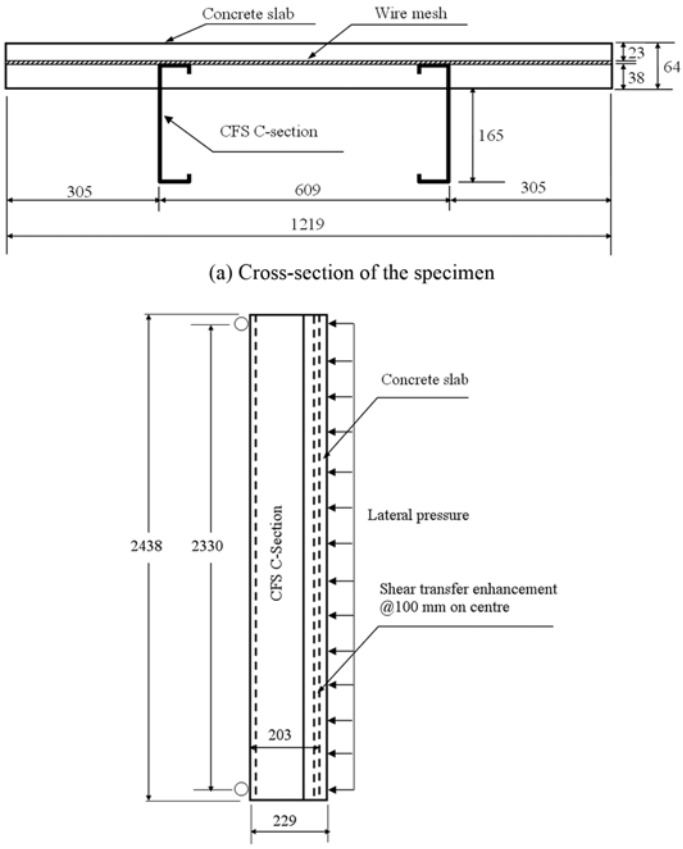

Fig. 1 Cross-section and elevation view of panel specimens (All dimension in mm)

restraint moment resulting from the specimen weight. The trolley roller system consisted of nine 13 mm diameter Stress-Proof® round bars with 830 MPa yield strength. In the direction of the lateral pressure (Fig. 5), the ends of the specimen acted against two lateral supporting W- shaped beams through steel round rods acting as roller supports. During mounting of a specimen, the rods were temporarily supported by two angles which were removed before testing. The ends of steel sections at the supports were reinforced with wood blocks fitted snugly between the C-section and the concrete slab. Bearing shoes built using hot-rolled steel flat bars were designed to provide against concrete bearing and to ensure smooth contact with the roller support.

Details of the instrumentation scheme are shown in Fig. 6. Two steel HSS columns were erected independently to the testing frame. Potentiometers were mounted on each column to measure deformations of the panel specimen through nylon monofilament strings attached to the measuring point on the concrete slab. For each specimen, six points of lateral displacement were monitored with three measured at each steel C-section location. Two of the three were measured at the end supports and one at the mid-height of a specimen. Four linear potentiometers placed at a location of 102 mm from each lateral support were used to measure the slip between the steel section and the concrete slab at those points.

Prior to testing, each specimen was cyclically preloaded three times using approximately 10% of the

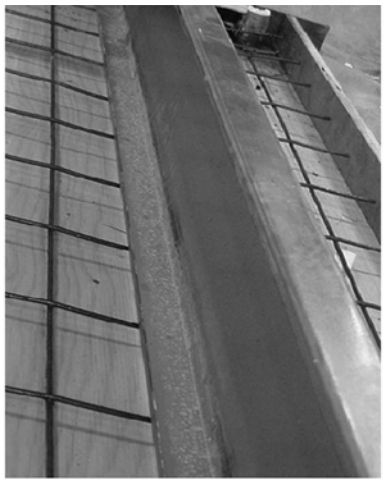

(a) Type A transfer mechanism- surface bond only

(b) Type B transfer mechanism- predrilled holes @ 100 mm on centre

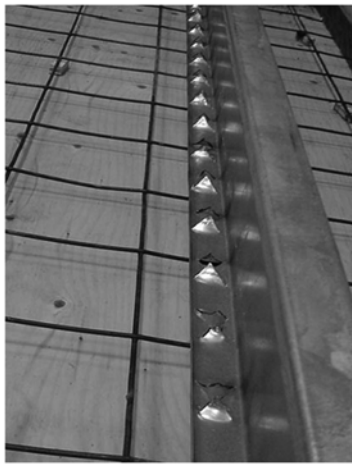

(c) Type C transfer mechanism- bent-up tabs @ 100 mm on centre

Fig. 2 Shear transfer mechanisms

expected ultimate load to ensure settling in of the specimen and the proper function of the instrumentation. The laterally applied airbag pressure was incremented gradually at a rate of 0.25 kPa/min for panel specimens with 41 mm × 152 mm C-sections, and 0.42 kPa/min for those stronger specimens with 41 mm × 203 mm C-sections. Load, slip and deflection readings were monitored and recorded using an electronic data acquisition system. Cracks on the concrete slab surface were mapped and noted with the load at which they occurred. Failure was deemed to have occurred when a specimen showed significant deflection and began to unload.

2.2 Push-out tests

Twenty push-out specimens were tested in seven series to determine the shear transfer capacity of

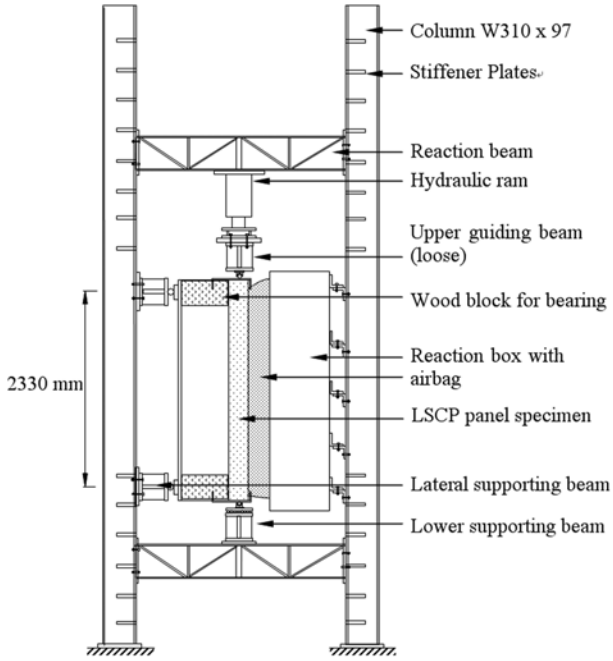

Fig. 3 Test set-up

three types of shear transfer mechanisms investigated in this research. Details of push-out specimens are summarized in Table 3. In the push-out tests, two 41 × 203 mm steel C-sections screw fastened together in a back-to-back configuration were used to ensure that the load was transferred through the centroid of the built-up section. As shown in Fig. 7, the flanges of this built-up section were embedded 38 mm into two nominally identical concrete plates measuring 406 mm wide, 64 mm deep, and 340 mm long. A recess of 40 mm in height was provided between the bottom of the column and the lower end of the steel section to allow for slip during testing. Series PO3 to PO7 included wire mesh to simulate the same condition as obtained in corresponding large-scale specimens whereas Series PO1 and PO2 did not have embedded mesh.

A 150 kN capacity Instron® testing machine was used to apply compressive load to each push out specimen through a stiff T-shaped wood block. Four LVDT displacement transducers, two on each side, were used to measure the slip at a distance 25 mm from the top end of the concrete plate and at 25 mm from the bottom of the steel section. The average of the readings from the four LVDTs was used to establish the shear resistance vs. slip relationship.

Before each test, specimens were subjected to two cycles of loading using a nominal compressive load of 5% of estimated ultimate load to ensure that the specimen and instrumentation were seated properly for testing. The rate of loading was synchronized with a rate of applied deflection of 0.6 mm/min. Testing was discontinued when the specimen failed to take additional load or when a significant load drop had occurred.

2.3. Material testing

Concrete cylinders, prepared at the same time as the casting of panels and push-out specimens, were

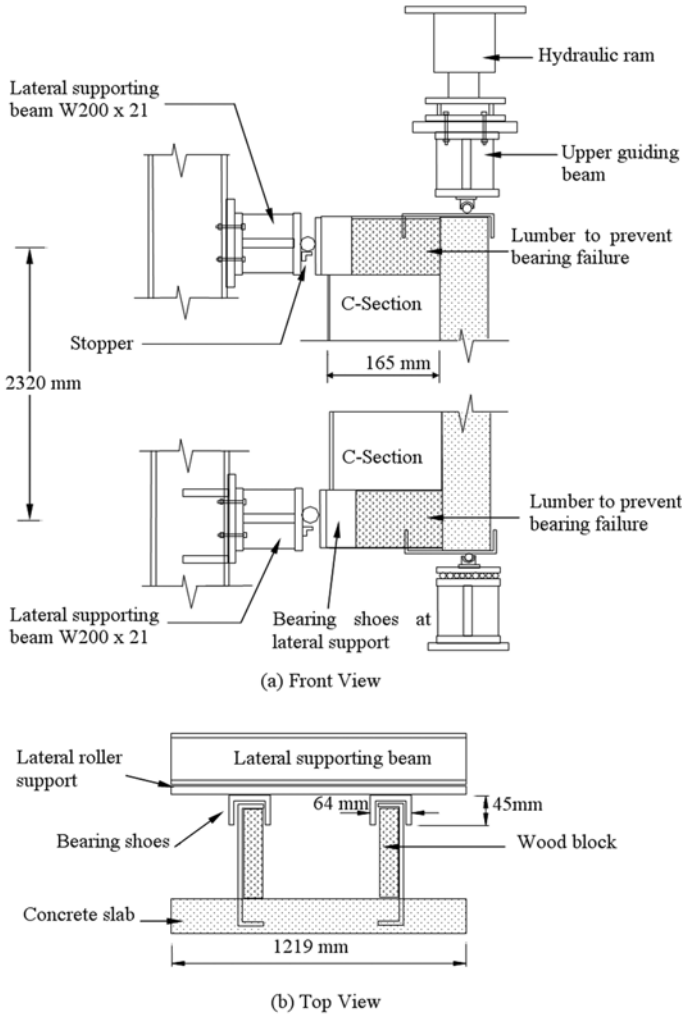

Fig. 4 Vertical support arrangement

cured under conditions similar to that of the full-size specimens. The compressive strength and the tension splitting strength of the concrete were determined according to ASTM standards (ASTM C39/C C39M-04 2004, ASTM C496/C496M-0412 2004). Coupons randomly cut from the web and flange of cold-formed steel C-sections were tested to determine the yield strength of the steel according to ASTM A370-03a (2004). All coupon specimens exhibited well defined yield plateau. Table 1 lists the compressive strength, f'_c, and tension splitting strength, f_t, of the concrete and the yield strength, f_y, of the steel for each specimen.

3. Test results and discussion

3.1 Panel specimens

A summary of test results of panel specimens is presented in Table 2, where p_u is the ultimate lateral

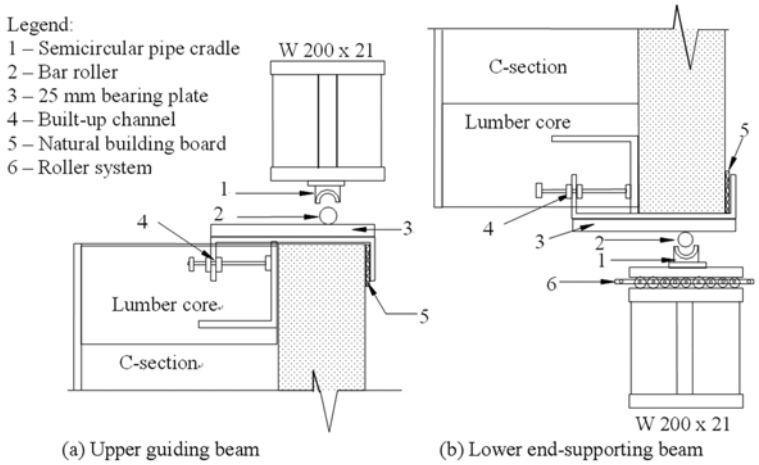

Fig. 5 Lateral support arrangement

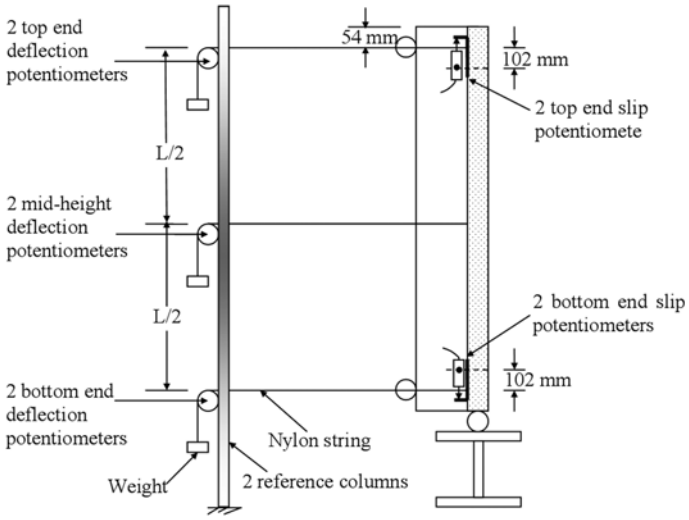

Fig. 6 Instrumentation scheme for panel specimens

pressure, δ_u is the slip at the interface of steel and concrete at the ultimate, Δ_u is the mid-height lateral deflection at the ultimate, p_s is the load corresponding to the allowable vertical deflection at the serviceability limit state, and p_{cr} is the load at which the first transverse crack was observed on the tension face of the concrete slab. The allowable deflection was taken as the limit, $L/360$, as specified in CSA S16.1-01 (2004) for floors supporting construction and finishes susceptible to cracking due to live load. This resulted in a limiting value of 6.4 mm for tested specimens. Table 2 shows that for all specimens, the values of p_{cr} were higher than those of p_s, indicating that at the serviceability limit state, no significant transverse cracking occurred in the concrete slab. On average, the first noticeable crack occurred at approximately 81% of the ultimate load whereas the serviceability load limit state was reached at about 70% of the ultimate load.

All specimens demonstrated similar failure modes. Failure was initiated by transverse cracking in the

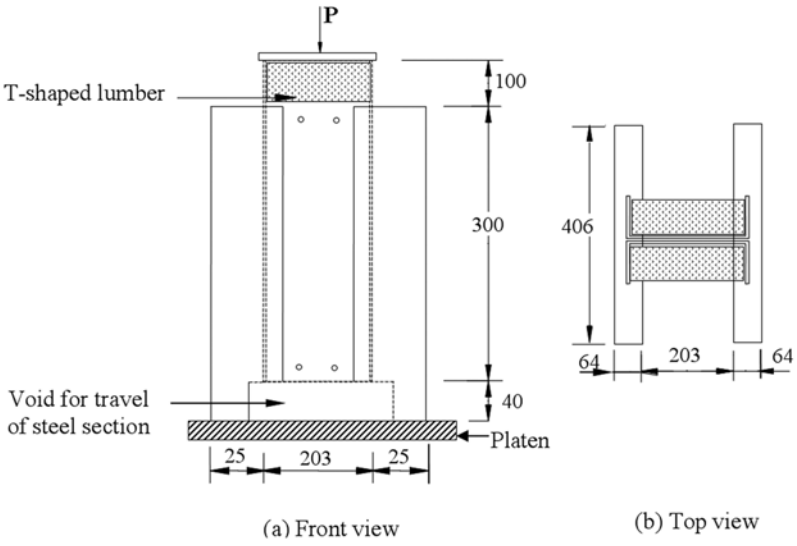

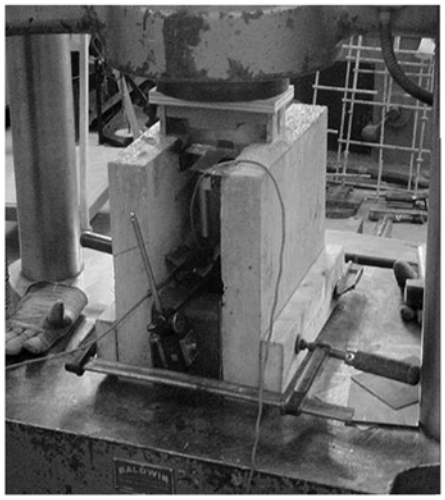

(c) Photographic view

Fig. 7 Description of the push-out specimen (All dimensions in mm)

concrete followed by tension yielding of the steel sections. At ultimate load, the cracks had progressed through the tension face of the concrete slab and extended over the entire width as crushing of the concrete at the bearings also occurred. The steel sections showed significant yielding with no sign of buckling. Distortion of the steel section in the form of folding over of the bottom flange towards the web was observed in almost all specimens after the ultimate load was reached. All specimens showed significant ductility and were, in most cases, able to maintain the ultimate load with increasing deflection until the load dropped. The deflection of the panel specimen and the transverse cracking observed on the bottom of the slab are illustrated in Fig. 8.

All specimens demonstrated similar behavior and a typical load vs. mid-height lateral deflection curve is shown in Fig. 9 for specimen LSCP 1. Up to the load level of p_s, which was about 70% of the

Table 2 Summary of test results for panel specimens

Specimen	Shear Connection	f'_c (MPa)	p_u (kPa)	δ_u (mm)	Δ_u (mm)	p_s (kPa)	p_{cr}(kPa)
LSCP1	Type A	33.8	35.5	1.47	81.1	25.3	27.8
LSCP2	Type B	33.8	43.2	0.43	61.4	32.1	34.6
LSCP3	Type C	33.8	42.2	0.50	68.5	30.5	34.7
LSCP4	Type B	36.6	44.2	0.37	73.0	34.3	39.2
LSCP5	Type B Greased	36.6	40.2	2.60	58.2	24.0	32.0
LSCP6	Type A	37.2	26.8	1.81	110.0	17.7	20.6
LSCP7	Type B	37.2	30.7	0.14	101.6	21.1	25.1
LSCP8	Type B	37.2	30.6	0.25	104.2	20.9	24.9

ultimate load, the response was linear. The first noticeable transverse crack was observed at about 80% of the ultimate load around the mid-height of the specimen and progressed with further increase in applied load. At the ultimate load, the transverse crack had extended over the entire width of the bottom face of the concrete slab and the steel C-section had fully yielded in the tension zone. The load vs. deflection response remained consistent for all specimens while specimens incorporating 41 × 203 mm C-sections attained an average of 36.8% higher ultimate capacity than those incorporating 41 × 152 mm C-sections. This is expected since the failure of all specimens was governed by tension yielding of the steel C-section. Therefore, the increase in the area of the C-section and thus the tension force in flexure provided a pronounced increase in the ultimate capacities of specimens.

3.1.1 Effect of shear transfer mechanisms

As seen in Table 2, the implementation of shear transfer enhancements resulted in greater values of all three loads, p_u, p_s, p_{cr}, and a reduction in both the slip and the lateral deflection when compared with surface bond only for shear transfer. For example, values of p_u, p_s, and p_{cr} for specimen LSCP2 with predrilled holes were 43.2 kPa, 31.1 kPa, and 34.6 kPa, respectively. These values represented increases of 22% above p_u of 35.5 kPa, 23% above p_s of 25.3 kPa, and 24% above p_{cr} of 27.8 kPa for specimen LSCP1 relying only on surface bond. The load vs. mid-height lateral deflection curves for specimens LSCP1 to LSCP3 are compared in Fig. 10. Specimens with shear transfer enhancement (LSCP2 and LSCP3) showed an average of 28% greater initial stiffness in the elastic range than the specimen relying only on surface bond for shear transfer (LSCP1). The onset of nonlinear behavior for specimen LSCP1 was observed around 27 kPa whereas the nonlinearity of responses for specimens LSCP2 and LSCP3 occurred around 34 kPa. Referring to values *of* p_s, these specimens behaved linear-elastically at serviceability limit states. The similarities in both the behavior and the ultimate loads of specimens LSCP2 and LSCP3 suggest that predrilled holes and bent-up cross-cut tabs had similar shear transfer performance and there was no clear advantage of one enhancement over the other.

Load vs. lateral deflection curves are plotted in Fig. 11 for specimens composite with 41 × 152 mm steel C-sections. Specimens LSCP7 and LSCP8 showed similar behavior and ultimate capacity, indicating that the test set-up was capable of delivering consistent results. The implementation of shear transfer enhancement resulted in a 35% increase in the initial stiffness for specimens LSCP7 and LSCP8 over specimen LSCP6 with surface bond only for shear transfer. A comparison in strength showed that specimens LSCP7 and LSCP8 attained increases of 14.1% in service load, 18% in cracking load, and 21% in ultimate load over specimen LSCP6.

(a) Transverse cracking on the bottom of the concrete slab

(b) Deflected shape of the panel specimen

Fig. 8 Failure mode of panel specimens

3.1.2 Effect of reduced bonding

A comparison of specimens LSCP4 and LSCP5 showed that specimen LSCP5 with debonding grease on the flange attained approximately 91% of the ultimate load, 80% of the service load, and 82% of the cracking load of its counterpart LSCP4 in which full bonding was permitted. The slip at the ultimate for specimen LSCP5 was 7 times that of specimen LSCP4. Experimental observations showed a visual separation between the steel section and the tension face of the slab at a load of 8.5 kPa for specimen LSCP5. Fig. 12 illustrates the responses for specimens LSCP4 and LSCP5 where specimen LSCP5 showed a 46.2% lower initial stiffness in the elastic range. This suggests that the lower initial stiffness resulting from reduced bonding had a greater effect on the service load than it had on the ultimate load. A comparison of surface bonded specimen LSCP1 with specimen LSCP5 with reduced bonding showed that specimen LSCP5

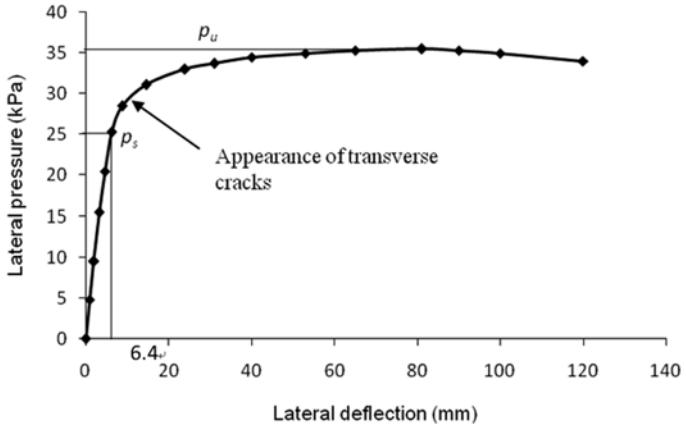

Fig. 9 A typical lateral load vs. lateral deflection curve (specimen LSCP1)

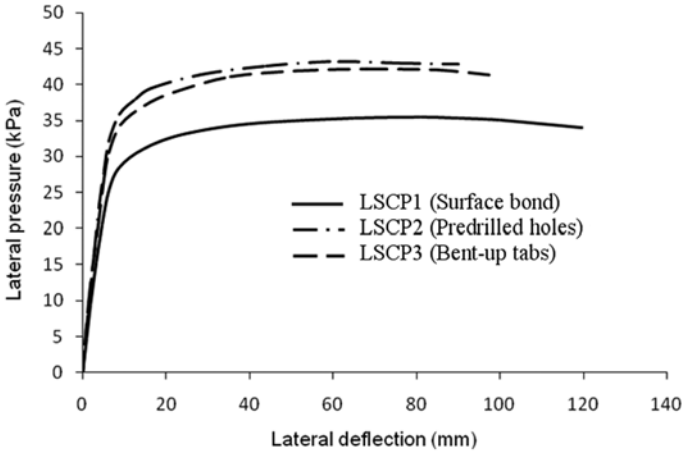

Fig. 10 Lateral load vs. lateral deflection curves (specimens LSCP1, LSCP2, and LSCP3)

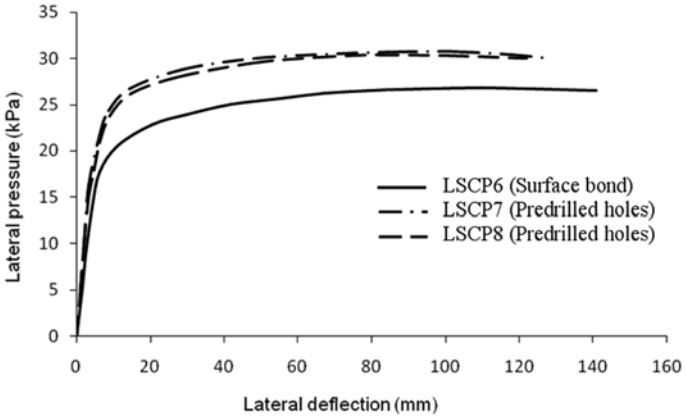

Fig. 11 Lateral load vs. lateral deflection curves (specimens LSCP6, LSCP7, and LSCP8)

attained an 11% higher ultimate load than specimen LSCP1. This higher capacity is attributed to both the concrete plugs formed by predrilled holes and the remaining surface bonding resistance after the application of the debonding grease. However, the service load p_s for specimen LSCP5 was less than that of specimen LSCP1 and the maximum slip for specimen LSCP5 was 1.8 times that of specimen LSCP1. This suggests that even with the shear transfer enhancement, the loss in surface bond had direct impact on the initial stiffness of the specimen and resulted in a relatively significant slip at the interface of steel and concrete.

3.1.3 Effect of concrete strength

The effect of concrete strength is illustrated in Fig. 13 where the behavior of specimen LSCP2 with a 33.8 MPa concrete was compared with specimen LSCP4 with a 36.6 MPa concrete. Both specimens demonstrated similar overall responses. For a difference of 8.3% in concrete strength, specimen LSCP4 showed a slightly higher initial stiffness and a 13.0% higher cracking load but a mere 2.3% higher ultimate capacity than that of specimen LSCP2. This indicates that higher strength concrete may have resulted in a delay in cracking but the failure of specimens was ultimately governed by the yielding of the steel section and therefore the concrete strength did not have a significant effect on the ultimate load.

3.2 Push-out tests

Results including the unit shear capacity, $q_{u(\mathrm{PO})}$, and the average of the measure slips, $\delta_{u(\mathrm{PO})}$, are presented in Table 3 for push-out specimens. The unit shear capacity was determined by dividing the ultimate load by the total embedded length of the flange of the steel section (1200 mm). The results presented were average values of specimens tested in each series. The coefficient of variation (C.O.V) of the results was determined to be 3.2%.

Three failure modes were observed for push-out specimens. Fig. 14a shows that for specimens without wire mesh (Series PO1 and PO2), longitudinal cracking began to develop at the lower end of the concrete plate and extended over its height before the maximum applied load was reached. For Series PO3 which included wire mesh but no shear transfer enhancement, failure occurred when the steel section was pushed through the concrete as shown in Fig. 14b. However, no visible cracking was observed. It is believed that the presence of wire mesh maintained the integrity of the concrete by preventing cracking. For those specimens having shear transfer enhancements (predrilled holes or bent-

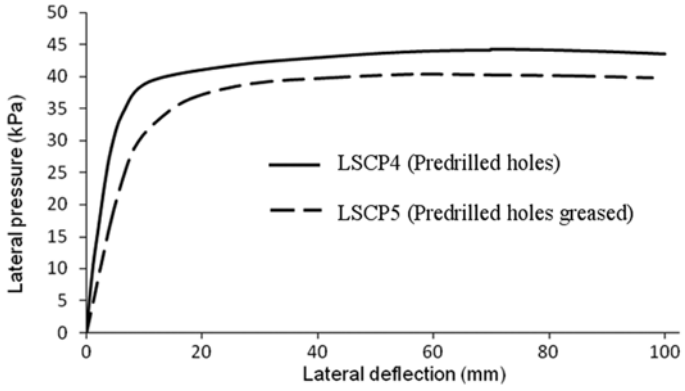

Fig. 12 Lateral load vs. lateral deflection curves (specimens LSCP4 and LSCP5)

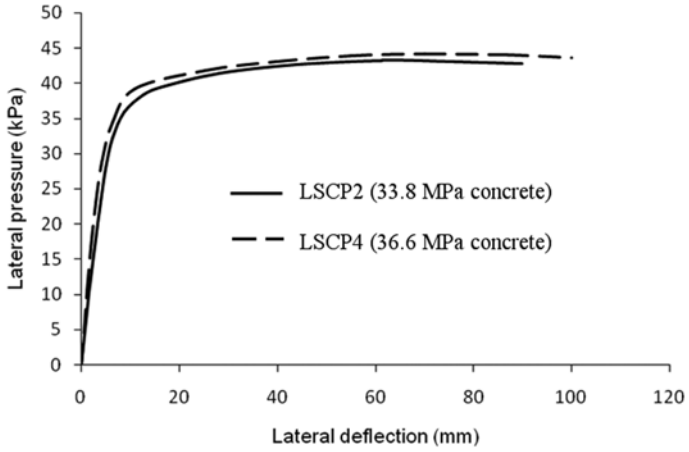

Fig. 13 Lateral load vs. lateral deflection curves (specimens LSCP2 and LSCP4)

up tabs) and the wire mesh, the failure is shown in Fig. 14c. The failure was initiated by a diagonal shear cracking formed at the top of the concrete. This longitudinal crack gradually extended over the height of the concrete and ultimately resulted in failure of the specimen. The combined effect of wire mesh and concrete plugs formed by predrilled holes or bent-up tabs were believed to result in the shear cracking. Similar failure modes were also noted by Lakkavali and Liu (2006). In most cases, the longitudinal crack appeared on both concrete plates whereas in some cases, the failure was confined to one side only.

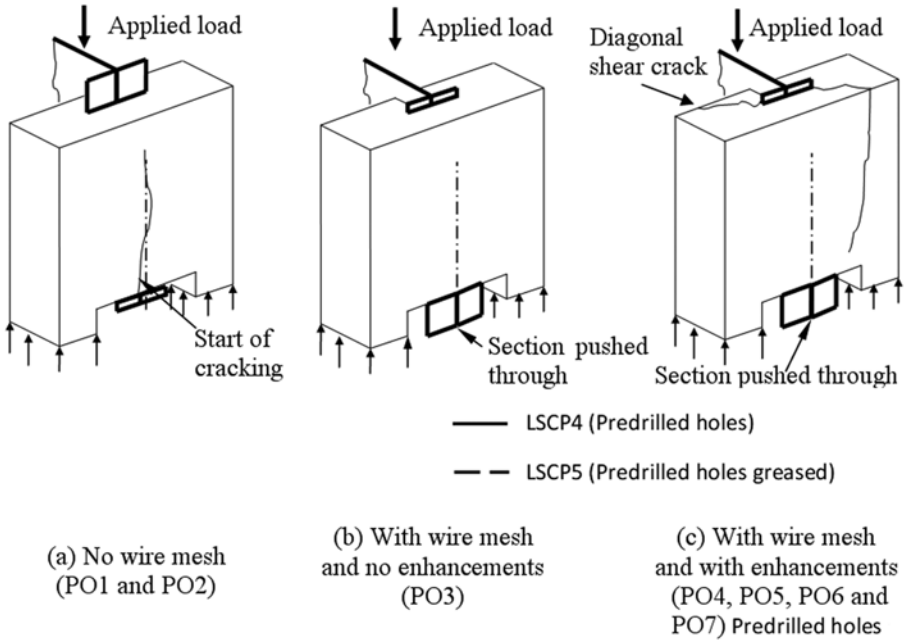

Fig. 14 Failure modes of push-out specimens

3.2.1 Effect of wire mesh

Table 3 shows that the inclusion of wire mesh in the concrete resulted in an increase in shear transfer capacity and a decrease in slip. Comparisons of capacities between Series PO1 and PO3 and between Series PO2 and PO4 showed that the presence of wire mesh increased the shear transfer resistance by approximately 19% in both instances. It suggests that the benefit of wire mesh in increasing the shear transfer resistance is similar in specimens with or without shear transfer enhancements.

3.2.2 Effect of shear transfer enhancements

Table 3 shows that whether or not the wire mesh was used, the predrilled holes on the embedded flange resulted in a significant increase in the shear transfer capacity ranging from 82 to 90% increase in comparison with surface bond only as indicated by comparisons of results of Series PO1 and PO2 and Series PO3 and PO4. The bent-up cross-cut tabs provided shear transfer capacity similar to that of the predrilled holes as indicated by the comparison of Series PO4 and PO5.

The contribution of predrilled holes to the shear transfer capacity can be quantitatively determined. In the case of Series PO1 and PO2 where no wire mesh was used, Series PO2 showed 31.6 kN/m more shear transfer whereas in the case of Series PO3 and PO4 where wire mesh was used, Series PO4 attained 41.4 kN/m more shear transfer. The increase in shear transfer was attributed to the shear resistance of concrete plugs formed by the predrilled holes, which amounted to shear resistances of 3.2 and 4.1 kN per hole, respectively. The shear transfer capacity of a concrete plug, S, may also be analytically evaluated using Eq. (1):

$$S = \frac{\pi d_h^2}{4} f_{ps} \tag{1}$$

where d_h is the diameter of the predrilled holes and f_{ps} is the shear strength of concrete assumed to be 20 % of the compressive strength (Pillai, *et al*. 1999).

Using Eq. (1), a 25.6 mm diameter concrete plug yielded a predicted shear capacity of 3.5 kN for a concrete compressive strength of 33.8 MPa, which was approximately the average of experimental values of 3.2 and 4.1 kN. It suggests that Eq. (1) provided a closer estimate of shear capacity of concrete plugs to the experimental value when the wire mesh was not used while markedly underestimated the shear capacity of concrete plugs when the wire mesh was used. The underestimation is believed to be attributed to the conservative approximation of shear strength of the concrete, f_{ps}, with the presence of

Table 3 Description of push-out specimens and test results

Series	Shear connection	No. of specimens	Wire mesh used	f'_c (MPa)	$q_{u(\mathrm{PO})}$ (kN/m)	$\delta_{u(\mathrm{PO})}$ (mm)
PO1	Type A	3	No	33.8	38.6	1.3
PO2	Type B	3	No	33.8	70.2	1.8
PO3	Type A	3	Yes	33.8	46.0	0.6
PO4	Type B	3	Yes	33.8	87.4	0.9
PO5	Type C	2	Yes	33.8	83.0	0.8
PO6	Type B	3	Yes	36.6	91.7	1.1
PO7	Type B Greased	3	Yes	36.6	71.4	0.8

wire mesh, although more experimental testing need to be conducted to verify this point.

3.2.3 Effect of reduced bonding

Bonding between the steel and the concrete was reduced by using a grease coating on the embedded flange of Series PO7. A comparison of Series PO6 and PO7 showed that the grease coated flange resulted in a reduction in the shear transfer capacity by about 22% from 91.7 kN/m for Series PO6 to 71.4 kN/m for Series PO7. To determine the loss in surface bonding due to grease coating, it was reasonably assumed that the shear resistance of the concrete plug formed by predrilled holes is not affected by the grease coating on the flange and it can be conservatively estimated using Eq. (1). For a one meter flange embedded in a 36.6 MPa concrete, the contribution of predrilled holes to the shear transfer was estimated to be 38.0 kN. The remaining contribution from the surface bond between the concrete and steel was then 53.7 kN for Series PO6 and 33.4 kN for Series PO7 specimens. This suggests that the grease coating resulted in a 38% loss of surface bonding, which led to the 22% reduction in the shear transfer capacity.

3.3 Summary

Results of panel specimens tested under uniform lateral pressure showed that all specimens failed in a ductile manner with significant lateral deflection. The values of cracking load when the first noticeable crack occurred were higher than those of service load for all specimens, indicating that in a design controlled by serviceability limit state, the behavior of studied LSCP panels would be in an elastic region. Specimens with shear transfer enhancements (predrilled holes and bent-up tabs) showed marked increases in initial stiffness, service load, cracking load and ultimate load when compared with specimens relying only on surface bond for shear transfer. Reduced bonding in specimens with predrilled holes resulted in reductions of various degrees in service load, cracking load and ultimate load of specimens but showing a greater effect on the service load than on the ultimate load. The variation of concrete strength did not show significant effect on the ultimate load of the specimen.

Push-out specimens were tested to evaluate the shear transfer capacity of individual shear transfer mechanisms. Results showed that the use of wire mesh resulted in a 19% increase in the shear transfer capacity by controlling longitudinal cracking of push-out specimens. Specimens with shear transfer enhancements attained more than 80% higher shear transfer capacity than surface bond specimens. The contribution of concrete plugs formed by predrilled holes to the shear capacity may be estimated using Eq. (1). Reduced bonding resulted in a 22% reduction in the shear transfer capacity of specimen with predrilled holes.

4. Correlation between push-out tests and panel specimen tests

The correlation between the results of push-out and panel specimens was studied and presented in Table 4. In the table, $M_{u(\mathrm{PS})}$ is the experimental ultimate moment obtained at the mid-height of the panel specimen; $Q_{u(\mathrm{PO})}$ is the shear transfer capacity based on the push-out tests and modified with respect to the shear span of the panel specimen; and $M_{u(\mathrm{PO})}$ is the calculated moment capacity of the large-scale specimen corresponding with $Q_{u(\mathrm{PO})}$. The shear capacity required for a full shear transfer, $V_{req'd}$, and the moment calculated based on a full shear transfer, $M_{u(\mathrm{full})}$ were also obtained. Procedures similar to those

described by Chien and Ritchie (1984) were used in the determination of both $M_{u(\mathrm{PO})}$ and $M_{u(\mathrm{full})}$ and a sample calculation of $M_{u(\mathrm{PO})}$ based on $Q_{u(\mathrm{PO})}$ is provided in Appendix A. For the calculation of forces provided by the steel C-section, it was assumed that tension yield strength was fully developed in the steel section before the ultimate moment was reached. Noting that, being embedded in the concrete, the compressive flange of the C-section is fully restrained against local or lateral buckling. It was therefore justified to consider the development of a plastic moment in the steel C-section.

The analysis shows that for all specimens, the shear capacity for a full transfer, $V_{req'd}$, was governed by the steel section yielding capacity, $A_s f_y$. As seen in the table, the experimental moment capacity $M_{u(\mathrm{PS})}$ was consistently greater than the calculated moment capacity $M_{u(\mathrm{PO})}$ based on the shear transfer resistance from the push-out tests. The ratio, $\frac{M_{u(PS)}}{M_{u(PO)}}$, had a mean value of 1.10 with a standard deviation of 0.02 for all tests. Similar observations were also made by other researchers (Slutter and Driscoll 1965, Johnson 1970, Oguejiofor and Hosain 1995, Lakkavalli and Liu 2006) indicating that push-out test results were conservative compared with those obtained from large-scale tests. This conservatism may be attributed to the difference in the application of loading in the two cases and the resulted failure modes. In push-out tests, the entire composite section was under concentric compression whereas in large-scale bending tests, the section was subject to strain gradient. At the interface between steel and concrete where the shear was transferred, strains did not reach the ultimate at the same time. The fibres with less strain may stabilize those subject to higher strains and therefore delay the failure and increase the strength.

The ratios of both $\frac{Q_{u(PO)}}{V_{req'd}}$ and $\frac{M_{u(PO)}}{M_{u(full)}}$ indicate that, except for specimens LSCP7 and LSCP8, partial shear transfer occurred for all specimens. For specimens with partial shear transfer, the percentage of transfer ranged from 41 to 85% and the corresponding moment capacity ranged from 83 to 97% of the ultimate moment capacity for full shear transfer. The specimen with shear transfer enhancements showed a higher percentage of shear transfer and therefore attained a moment capacity closer to that for a fully composite panel. It is worthwhile to note that even for specimens LSCP1 and LSCP6, which relied on surface bond to transfer shear, ultimate moment capacities still reached 83% and 88%, respectively, of a full composite panel. Referring to Table 3, the slip measured at the steel and concrete interface is directly associated with the shear transfer percentage. A low percentage of shear transfer corresponded consistently with a high magnitude of slip. Specimens LSCP7 and LSCP8 composite with 41 × 152 mm C-sections showed a 99% shear transfer and the lowest slip values among all specimens. This suggests that for the

Table 4 Comparison of push-out and panel specimen tests

Specimen	$M_{u(\mathrm{PS})}$ (kN-m)	$Q_{u(\mathrm{PO})}$ (kN)	$M_{u(\mathrm{PO})}$ (kN-m)	$\frac{M_{u(PS)}}{M_{u(PO)}}$	$V_{req'd}$ (kN)	$\frac{Q_{u(PO)}}{V_{req'd}}$	$M_{u(\mathrm{full})}$ (kN-m)	$\frac{M_{u(PO)}}{M_{u(Pull)}}$
LSCP1	29.1	55.7	27.1	1.07	131.9	0.42	32.7	0.83
LSCP2	35.4	107.2	31.6	1.12	131.9	0.81	32.7	0.97
LSCP3	34.6	101.8	31.4	1.10	131.9	0.77	32.7	0.96
LSCP4	36.3	112.4	32.1	1.13	132.5	0.85	32.9	0.97
LSCP5	33.0	87.5	30.9	1.07	132.5	0.66	32.9	0.94
LSCP6	22.0	58.3	20.0	1.10	114.5	0.51	22.8	0.88
LSCP7	25.2	113.3	22.8	1.11	114.5	0.99	22.8	1.00
LSCP8	25.1	113.3	22.8	1.10	114.5	0.99	22.8	1.00

given geometry and material characteristics, the use of a steel section whose yield capacity was close to the shear transfer capacity resulted in a nearly full composite panel.

5. Conclusions

Eight composite panel specimens incorporating light gage steel C-sections and twenty companion push-out specimens were tested to investigate the efficacy of various shear transfer mechanisms. The following conclusions may be drawn from the study:

1. All specimens with shear transfer mechanisms investigated herein, when tested under uniform lateral pressure, exhibited good serviceability and ductility characteristics.
2. The implementation of shear transfer enhancements resulted in, on average, an 31% increase in initial stiffness, 86% increase in shear transfer capacity and a 17% increase in ultimate moment capacity over specimens relying only on surface bond.
3. Reduced bonding in specimens with predrilled holes resulted in a higher reduction in service load of the specimen than in its ultimate load.
4. The presence of wire mesh resulted in an increase in the shear transfer capacity and a reduction in slip in push-out specimens.
5. The calculated moment capacity based on shear transfer resistance obtained from push-out tests is, on average, 10% lower than the experimental ultimate capacity of the specimen.
6. Specimens relying only on surface bond for shear transfer achieved partial transfer of 42 to 51% with corresponding moment capacities ranging from 83 to 88% of that for a full composite specimen. Specimens with shear transfer enhancements realized a 77 to 99% shear transfer with the corresponding moment capacities ranging from 95 to 100%.
7. Specimens incorporating 41 × 152 mm steel C-sections with 25 mm predrilled holes as shear transfer enhancement achieved almost 100% shear transfer.

In summary, the shear transfer mechanism consisting of surface bonding in conjunction with predrilled holes in the embedded flanges of the steel C-section resulted in the highest ultimate load. Its simplicity, effectiveness and economy of manufacture make it the most industrially viable. In order to establish the shear capacity of such shear enhancement in a closed form equation for design, it is recommended that more experimental testing be conducted to include parameters such as the diameter and spacing of the holes, concrete strength and wire mesh characteristics.

Appendix A. Sample calculation of predicted capacity: LSCP1

Slab span: L = 2330 mm

Steel section properties:

C-section: 1.504 mm thick

Area: A_s = 440.0 mm^2

f_y = 299.8 MPa;

Concrete slab properties (making use of symmetry, a half cross-section is analyzed as shown in Fig. A1):

b_1 = 609 mm

t_1 = 64 mm

t_{1f} = 26 mm

f'_c = 33.8 MPa;

Push-out specimen details:

Ultimate load of push-out specimen $q_{u(PO)}$ = 46 kN/m

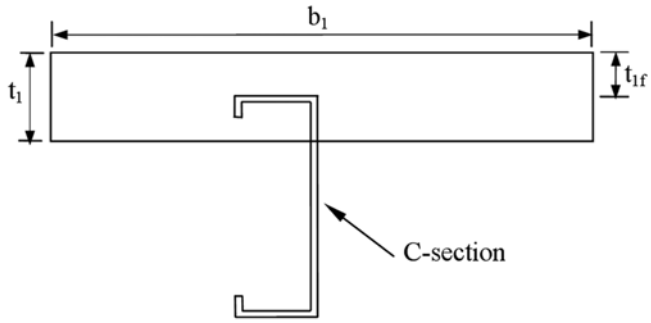

Fig. A1 Half cross-section details

Total shear transfer capacity provided in one shear span of the flexural specimen:
$Q_{u(PO)}$ = 55.7 kN
Maximum horizontal shear at steel-to-concrete interface, V_h:
V_h is the lesser of 0.85 f'_c $b_1 t_{1f}$ and $A_s f_y$:
(i) 0.85 f'_c $b_1 t_{1f}$ = 0.85 × 33.8 × 609 × 26 = 454.9 kN
(ii) $A_s f_y$ = 456.77 × 299.8 = 131.9 kN.
Therefore,
V_h = 131.9 kN.
Since $Q_{u(PO)} < V_h$, shear transfer is partial.
Referring to Fig. A2, the maximum compressive force in the concrete slab $C_c = Q_{u(PO)}$ = 55.7kN.
Depth of concrete stress block to support C_c is given by:

$$a = \frac{C_c}{0.85 f'_c b_1} = \frac{55.7 \times 10^3}{0.85 \times 33.8 \times 609} = 3.2 \text{ mm}$$

For equilibrium, $T_r = A_s f_y - C_r = C_c + C_r$;

$$C_r = \frac{A_s f_y - C_c}{2} = \frac{(131.9 - 55.7) \times 10^3}{2} = 38.1 \text{ kN}$$

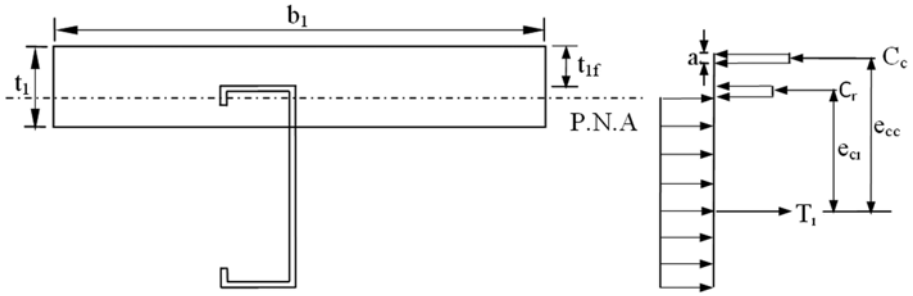

Fig. A2 Stress distribution in composite sectiion

Maximum compressive force in the steel section top flange:

$C_{rf} = b_t f_y = 41.3 \times 1.504 \times 299.8 = 18.6$ kN

$C_r > C_{rf}$.

Plastic neutral axis lies within the web as shown in Fig. A3.

Depth of the plastic neutral axis from the top of the flange is given by:

$$1.504 + \frac{(38.1 - 18.6) \times 10^3}{2 \times 1.504 \times 299.8} = 23.4 \text{ mm}$$

The centroid locations of the tensile portion and the compressive portion of the C-section are obtained as follows:

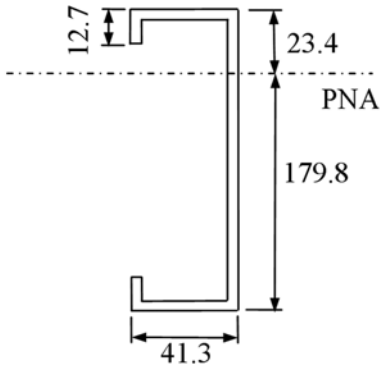

Fig. A3 Determination of centroids of C-section

Compressive portion (measured from top flange): 4.9 mm.

Tensile portion (measured from bottom flange): 71.2 mm.

The lever arms e_{cc} and e_{cr} are given by

$$e_{cc} = 203.2 + 26 - 71.2 - \frac{3.2}{2} = 156.3 \text{ mm}$$

$e_{cr} = 203.2 - 4.9 - 71.2 = 127.1$ mm.

Hence, the ultimate flexural capacity, $M_{u(\text{PO})}$ for the full cross section based on push-out specimen results, is given by

$M_{u(\text{PO})} = 2 \times (C_c e_{cc} + C_r e_{cr})$

$= 2 \times (55.7 \times 156.3 + 38.1 \times 127.1)$

$= 27.1$ kN-m.

References

AASHTO LRFD Bridge Design Specifications (2005), *American Association of State Highway and Transportation Officials*, 3rd ed., Washington, DC.

ASCE Specification for the design and construction of composite slabs (1984), New York, NY.

ASTM A370-03 (2004), *Standard test methods and definitions for mechanical testing of steel products*, Annual book of ASTM standards, vol. 01.04.
ASTM C39/C C39M-04 (2004), *Standard test method for compressive strength of cylindrical concrete specimens*, Annual Book of ASTM standards, vol. 04.02.
ASTM C496/C496M-04 (2004), *Standard test method for splitting tensile strength of cylindrical concrete specimens*, Annual Book of ASTM standards, vol. 04.02.
Badie, S.S., Tadros, M.K., Kakish, H.F., Splittgerber, D.L. and Baishya, M.C. (2002), "Large shear studs for composite action in steel bridge girders", *J. Bridge Eng.*, **7**(2), 195-203.
CAN/CSA-S136-01 (2001), *Cold formed steel structural members*, National Standard Code of Canada, Ontario.
CAN/CSA-S16.1-01 (2004), *Limit States Design of Steel Structures*, 8th ed., Canadian Institute of Steel Construction, Willowdale, ON, Canada.
Chien, E.Y.L. and Ritchie, J.K. (1984), *Design and Construction of Composite Floor Systems*, Canadian Institute of Steel Construction, Ontario, Canada.
Culver, C. and Coston, R. (1961), "Tests of composite beams with stud shear connectors", *J. Struct. Div.* ASCE, **87**(ST2), 1-17.
Ekberg, C.E. and Schuster, R.M. (1968), "Floor systems with composite from reinforced concrete slabs", Final report, IABSE New York.
El-Lobody, E. and Lam, D. (2002), "Modelling of headed stud in steel-precast composite beams", *Steel Compos. Struct.*, **2**(5), 355-378.
Erdélyi, S. and Dunai, L. (2009), "Light-gauge composite floor beam with self-drilling screw shear connector: experimental study", *Steel Compos. Struct.*, **9**(3), 255-274.
Greiner, R., Ofner, R. and Unterweger, N.H. (2002), "Composite deck construction for the rehabilitation of motorway bridges", *Steel Compos. Struct.*, **2**(1), 67-84.
Hanaor, A. (2000), "Tests of composite beams with cold-formed sections", *J. Constr. Steel Res.*, **54**(3), 245-264.
Johnson, R.P. (1970), "Research on steel concrete composite beams", *J. Struct. Div.* ASCE, **96**(ST3), 445-459.
Lakkavalli, B.S. and Liu, Y. (2006), "Experimental study of composite cold-formed steel C- section floor joists", *J. Constr. Steel Res.*, **62**(5), 995-1006.
Oguejiofor, E.C. and Hosain, M.U. (1995), "Tests of full size beams with perfobond rib connectors", *Can. J. Civil Eng.*, **22**(1), 80-92.
Pillai, S.U., Kirk, D.W. and Erki, M.A. (1999), *Reinforced concrete design*, 3rd edition, McGraw-Hill Ryerson, Whitby, ON, Canada.
Porter, M.L. and Ekberg, C.E. (1976), "Design recommendations for steel deck floor slabs", *J. Struct. Div.* ASCE, **102**(ST11), 2121-2136.
Slutter, R.G. and Driscoll, G.C. (1965), "Flexural strength of steel-concrete composite beams", *J. Struct. div.* ASME, **91**(ST2), 71-99.
United States Patent and Trademark Office (2003), *Database of United States Patent and Trademark Office*, http://www.uspto.gov/patft.

CE

Notation

a	Depth of concrete stress block in compression (mm)
A_s	Area of steel channel section (mm^2)
b_l	Width of concrete slab being analyzed (mm)
b_t	Width of flange of steel C-section (mm)
C_c	Compressive force provided by the concrete slab (kN)
C_r	Compressive forced provided by the steel section (kN)
C_{rf}	Compressive force provided by the flange of the steel section (kN)

d_h	Diameter of predrilled holes in embedded steel flange (mm)
e_{cc}	Moment arm of the compressive force C_c (mm)
e_{cr}	Moment arm of the compressive force C_r (mm)
f'_c	Compressive strength of concrete (MPa)
f_{ps}	Pure shear strength of concrete (MPa)
f_t	Splitting strength of concrete (MPa)
f_y	Tensile yield strength of steel (MPa)
L	Span of panel (mm)
$M_{u(PS)}$	Experimental moment capacity of panel specimen (kN-m)
$M_{u(PO)}$	Calculated moment capacity based on push-out shear transfer resistance (kN-m)
$M_{u(full)}$	Calculated moment capacity based on a full shear transfer (kN-m)
p_{cr}	Lateral pressure at the first crack of large-scale specimen (kPa)
p_s	Lateral pressure corresponding to the serviceability limit state (kPa)
p_u	Ultimate lateral pressure of large-scale specimen (kPa)
$q_{u(PO)}$	Unit shear transfer capacity from push-out tests (kN/m)
$Q_{u(PO)}$	Shear transfer capacity from push-out tests for large-scale specimen (kN)
S	Shear resistance provided by each predrilled hole (kN)
t_1	Thickness of the concrete slab (mm)
t_{1f}	Thickness of the concrete slab above the embedded flange of the steel section (mm)
V_h	Shear transferred at the steel and concrete interface
$V_{req'd}$	Shear transfer capacity required for a full transfer (kN)
Δ_u	Mid-height lateral deflection at the ultimate (mm)
δ_u	Maximum slip at the interface of steel and concrete for large-scale specimen (mm)
$\delta_{u(PO)}$	Average value of measured slips at ultimate for push-out specimen (mm)